

# The Practicality of Normalizing Flow Test-Time Training in Bayesian Inference for Agent-Based Models

Junyao Zhang, Jinglai Li, Junqi Tang

School of Mathematics, University of Birmingham

January 12, 2026

## Abstract

Agent-Based Models (ABMs) are gaining great popularity in economics and social science because of their strong flexibility to describe the realistic and heterogeneous decisions and interaction rules between individual agents. In this work, we investigate for the first time the practicality of test-time training (TTT) of deep models such as normalizing flows, in the parameters posterior estimations of ABMs. We propose several practical TTT strategies for fine-tuning the normalizing flow against distribution shifts. Our numerical study demonstrates that TTT schemes are remarkably effective, enabling real-time adjustment of flow-based inference for ABM parameters.

## 1 Introduction

Agent-Based Models (ABMs) provide an important modelling paradigm in the study of economics, financial markets, and broader complex systems [4, 5, 6]. Thanks to the expressiveness of ABMs to describe realistic and heterogeneous decisions and interaction rules between agents, these models allow modellers to analyze the whole systems mechanistically with respect to individual agents. Specifically, ABMs generally take parameters  $\theta \in \Theta \subset \mathbb{R}^d$  as input, and return time-series data  $x_t$ . However, ABMs are stochastic estimators, that is, given fixed parameters  $\theta$ , models will produce different output  $x$  between each run, which are drawn from the conditional probability density function  $p(x | \theta)$ .

The key of successfully applying ABMs to real-world problems is to perform parameter inference of  $\theta$ . Nevertheless, due to strong nonlinearity, heterogeneous agent interactions and complex feedback mechanisms, the likelihood  $p(x | \theta)$  is generally intractable for random estimators, making classical maximum likelihood estimation infeasible and leading to a likelihood-free inference problem.

To address this challenge, many relative works have been extensively developed in recent years, among which Neural Posterior Estimation (NPE), a simulation-based Bayesian inference technique, is a prominent approach. The core idea of the NPE application to ABMs is to train a neural network to approximate the posterior distribution of parameters  $q_\phi(\theta | x)$  directly by first drawing parameter samples  $\theta^{(i)} \sim p(\theta)$ , generating simulated data  $x^{(i)} \sim p(x^{(i)} | \theta^{(i)})$ , and then, to make the learned distribution approaches the true posterior density directly.

In practice, the density estimator  $q_\phi$  is commonly parameterised using *normalizing flows* [11, 9, 2, 12]. A normalizing flow defines an expressive distribution by transforming a simple base

distribution through a sequence of invertible and differentiable mappings  $\{f_{\phi_i}\}_{i=1}^n$  with trainable parameters  $\phi_i$ , where  $\phi = (\phi_n, \dots, \phi_1)$ . The resulting density estimator  $q_\phi$  can be written as

$$q_\phi(\mathbf{x}) = p_{\mathbf{U}}\left(f_{\phi_1}(\cdots f_{\phi_{n-1}}(f_{\phi_n}(\mathbf{x}))\cdots)\right) \left| \prod_{i=1}^n \det J_{f_{\phi_i}}(\mathbf{x}) \right|, \quad (1)$$

where  $J_{f_{\phi_i}}(\mathbf{x})$  denotes the Jacobian matrix of the transformation  $f_{\phi_i}$  evaluated at  $\mathbf{x}$ .

Normalizing flows offer strong expressiveness for non-linear posteriors inference, but this expressiveness incurs substantial computational cost. Specifically, in NPE, high-dimensional parameter spaces require complex invertible transformations, multi-layer flows demand repeated Jacobian evaluations, and relatively large simulation budgets are needed for stable training. Consequently, once the parameters distribution environment of an ABM shifts, retraining a full normalizing flow-based NPE model becomes computationally expensive.

To mitigate this computational burden, in this paper, we investigate several strategies in the Test-Time Training [14, 13] for the first time, to fine-tune the pre-trained posterior estimator to a new model with parameter distribution shift, rather than retraining the full normalizing flow. Firstly, we employ traditional test-time training strategies, full parameters fine-tuning and parameter-efficient low-rank adaptation (LoRA) [7], which updates all network parameter and restricts network weight to a low-dimensional subspace, respectively. Using the numerical experiments in Brock-Hommes model as an example, although LoRA has slightly worse performance caused by the zero initialization, these two approaches enable efficient posterior correction across distribution shift while avoiding the expensive retraining of the full flow-based estimator.

To further achieve parameter-efficient test-time training in the parameter posterior inference of ABMs, we propose two methods based on the gradient subspace. The core idea underlying them is using only a small amount of target-task data to identify a low-dimensional adaptation subspace around the pre-trained parameters and then constraining optimization to this subspace [3, 8, 15, 10]. On this basis, *GradSubspace-TTT* uses backward hook to project each step of backward propagation into this subspace so that it can restrict every update to high-information directions, and *GradSubspace-PEA* reparameterises the model as  $\phi = \phi_0 + U_r c$  and optimises only the low-dimensional coefficients  $c$ , achieving parameter efficiency with minimal optimiser state. Our numerical experiments in Brock-Hommes model demonstrate this two methods based on gradient subspace providing an objective-directed alternative yielding efficient and stable posterior correction in distribution shift.

## 2 Neural Posterior Estimation

In this section, we provide an overview of Neural Posterior Estimation (NPE), one of the most prominent simulation-based inference method, and its application in ABMs [4]. The core idea underlying NPE is to employ neural networks to approach the parameter posterior density directly via neural conditional density estimators, such as normalizing flow.

### 2.1 Normalizing Flow

Normalizing flows have capacity of constructing a flexible density by transforming a simple base distribution into a sophisticated one using neural networks. Given a random variable  $\mathbf{U} \sim p_{\mathbf{U}}$  following a simple distribution, that is, we can sample from  $p_{\mathbf{U}}$  and evaluate  $p_{\mathbf{U}}(u)$  for any  $u$  easily, and define  $\mathbf{X} = g(\mathbf{U})$  where  $g$  is bijective with inverse  $f := g^{-1}$ . By the change of variables formula,

the induced density is

$$p_{\mathbf{X}}(\mathbf{x}) = p_{\mathbf{U}}(f(\mathbf{x})) |\det J_f(\mathbf{x})|, \quad (2)$$

where  $J_f$  denotes the Jacobian of  $f$ . Sampling from  $p_{\mathbf{X}}$  is therefore straightforward by drawing  $\mathbf{u} \sim p_{\mathbf{U}}$  and setting  $\mathbf{x} = g(\mathbf{u})$ . Density evaluation can be obtained from the right-hand side of Equation (2) by given  $\mathbf{x}$ , computing  $\mathbf{u} = f(\mathbf{x})$  and the Jacobian determinant term. Practically we can take a simple composition  $g = g_n \circ g_{n-1} \circ \dots \circ g_1$ , to construct a flow, so that one can iteratively transform  $\mathbf{u}_0 = \mathbf{u} \sim p_{\mathbf{U}}$  via  $\mathbf{u}_i = g_i(\mathbf{u}_{i-1})$  to obtain  $\mathbf{x} = \mathbf{u}_n$ , and evaluate densities by applying the inverses  $f_i$  in reverse order while accumulating the corresponding Jacobian determinants, for which we now have Equation (1)

$$q_{\phi}(\mathbf{x}) = p_{\mathbf{U}}\left(f_{\phi_1}(\dots f_{\phi_{n-1}}(f_{\phi_n}(\mathbf{x}))\dots)\right) \left| \prod_{i=1}^n \det J_{f_{\phi_i}}(\mathbf{x}) \right|,$$

Given data samples  $\mathbf{x}^{(r)} \stackrel{\text{iid}}{\sim} p_{\mathbf{X}}$ , the learnable parameters  $\phi = \{\phi_i : 1 \leq i \leq n\}$  of the flows are optimized by maximum log-likelihood:

$$\hat{\phi} = \arg \max_{\phi} \sum_{r=1}^R \log q_{\phi}(\mathbf{x}^{(r)}). \quad (3)$$

## 2.2 Neural Posterior Estimation Based on Normalizing Flow

Normalizing flows can also be extended to *conditional* density estimation. In the ABMs setting, this enables us to model the posterior directly with a conditional flow  $q_{\phi}(\boldsymbol{\theta} \mid \mathbf{x})$  where the flow transformation parameters are produced by a neural network. Training proceeds by maximising log-likelihood on simulated joint pairs  $(\mathbf{x}^{(r)}, \boldsymbol{\theta}^{(r)})$  generated from  $p(\mathbf{x}, \boldsymbol{\theta}) = p(\boldsymbol{\theta}) p(\mathbf{x} \mid \boldsymbol{\theta})$ ,  $r = 1, \dots, R$ , yielding the estimator

$$\hat{\phi} = \arg \max_{\phi \in \Phi} \sum_{r=1}^R \log q_{\phi}(\boldsymbol{\theta}^{(r)} \mid \mathbf{x}^{(r)}). \quad (4)$$

A key advantage of this conditional-flow formulation is that it learns a *single* amortised posterior estimator across different  $\mathbf{x}$ , rather than training a separate density estimator for each fixed observation when evaluating the posterior.

## 2.3 Sequential Neural Posterior Estimation

In previous section, we introduce the standard one-stage NPE and its application in posterior inference in ABMs. A practical limitation is that, for a fixed observation  $\mathbf{x}$ , most prior-drawn parameters produce simulations far from the posterior support, leading to wasted simulation budget.

Therefore, it is necessary to introduce round-based *Sequential Neural Posterior Estimation (SNPE)* procedure that progressively focuses simulations on parameter regions relevant to  $\mathbf{x}$ . Let  $\tilde{p}_m(\boldsymbol{\theta})$  denote the proposal used at round  $m$ , with initialization  $\tilde{p}_0(\boldsymbol{\theta}) = p(\boldsymbol{\theta})$ . At each round, we simulate

$$\boldsymbol{\theta}^{(n)} \stackrel{\text{iid}}{\sim} \tilde{p}_m(\boldsymbol{\theta}), \quad \mathbf{x}^{(n)} \sim p(\mathbf{x} \mid \boldsymbol{\theta}^{(n)}),$$

append the resulting pairs to the training set, and then retrain learnable network parameters. A common choice is to set the next proposal to the current posterior estimate at the target observation,

$$\tilde{p}_{m+1}(\boldsymbol{\theta}) := q_{\phi}(\boldsymbol{\theta} \mid \mathbf{y}),$$

so that successive rounds concentrate simulations around high-posterior-mass regions.

Because from round  $m \geq 1$  the training data are no longer drawn from the prior joint  $p(\mathbf{x}, \boldsymbol{\theta})$ , the likelihood objective must correct for proposal sampling. It can be expressed by using a weighted objective:

$$\mathcal{L}(\phi) = - \sum_{(\mathbf{x}, \boldsymbol{\theta}) \in \mathcal{D}} \log \left( q_\phi(\boldsymbol{\theta} | \mathbf{x}) \frac{\tilde{p}_m(\boldsymbol{\theta})}{p(\boldsymbol{\theta})} \frac{1}{Z(\mathbf{x}, \phi)} \right), \quad (5)$$

where  $Z(\mathbf{x}, \phi)$  is a normalizing factor ensuring the expression integrates to one over  $\boldsymbol{\theta}$ . We employ SNPE to learn the posterior distribution of parameters in ABMs as described in Algorithm 1.

---

**Algorithm 1** Sequential Neural Posterior Estimation

---

**Input:** Prior distribution  $p(\theta)$ , simulator  $p(x | \theta)$ , observation  $y$ , conditional density estimator  $q_\phi(\theta | x)$ , number of rounds  $M$ , number of simulations per round  $N$ .

Initialize proposal  $\tilde{p}_0(\theta) = p(\theta)$ .

Initialize dataset  $\mathcal{D} = \{\}$ .

**for**  $m = 0, \dots, M - 1$  **do**

    Sample parameters  $\theta_n^{(m)} \sim \tilde{p}_m(\theta)$  for  $n = 1, \dots, N$ .

    Simulate data  $x_n^{(m)} \sim p(x | \theta_n^{(m)})$ .

    Append dataset:

$$\mathcal{D} := \mathcal{D} \cup \bigcup_{n=1}^N \{(x_n^{(m)}, \theta_n^{(m)})\}.$$

**SNPE training step**

**while** not converged **do**

    Evaluate loss:

$$\mathcal{L}(\phi) = - \sum_{(\mathbf{x}, \boldsymbol{\theta}) \in \mathcal{D}} \log \left( q_\phi(\boldsymbol{\theta} | \mathbf{x}) \frac{\tilde{p}_m(\boldsymbol{\theta})}{p(\boldsymbol{\theta})} \frac{1}{Z(\mathbf{x}, \phi)} \right).$$

    Update trainable parameters  $\phi$  using  $\nabla_\phi \mathcal{L}(\phi)$ .

**end while**

    Set new proposal distribution:

$$\tilde{p}_{m+1}(\theta) := q_\phi(\theta | y).$$

**end for**

---

### 3 Brock–Hommes Model

In the numerical experiment, we evaluate SNPE-TTT, SNPE-LoRA and Gradient-Based Test-Time Training on the foundation of a variant of the model proposed by Brock and Hommes in 1998 [1]. This Agent-Based Model describes heterogeneous agents affect asset pricing in which prices evolve based on forecasts made by different trader types. The model generates various nonlinear dynamics, including periodicity, excess volatility, and chaotic behavior.

### 3.1 Introduction to Brock-Hommes Model

The variable of interest  $x_t$  denotes the deviation of the asset price from its fundamental value. Agents choose trading strategies adaptively. The fraction of type  $h$  traders at time  $t+1$  is determined through a discrete-choice model, based on past performance. Its evolution is governed by

$$x_{t+1} = \frac{1}{R} \left[ \sum_{h=1}^H n_{h,t+1} (g_h x_t + b_h) + \varepsilon_{t+1} \right], \quad \varepsilon_{t+1} \sim \mathcal{N}(0, \sigma^2), \quad (6)$$

$$n_{h,t+1} = \frac{\exp(\beta(x_t - Rx_{t-1})(g_h x_{t-2} + b_h - Rx_{t-1}))}{\sum_{k=1}^H \exp(\beta(x_t - Rx_{t-1})(g_k x_{t-2} + b_k - Rx_{t-1}))}, \quad (7)$$

where  $R = 1 + r$  is the gross interest rate,  $g_h$  represents the strength of trend-following,  $b_h$  represents belief or bias, and  $\beta > 0$  controls sensitivity to strategy profitability.

In our setting, the number of trader types is  $H = 4$ . Parameters for types 1 and 4 are fixed as

$$g_1 = b_1 = b_4 = 0, \quad g_4 = 1.01,$$

and the goal is to infer the posterior distribution of remaining four parameters

$$\theta = (g_2, b_2, g_3, b_3).$$

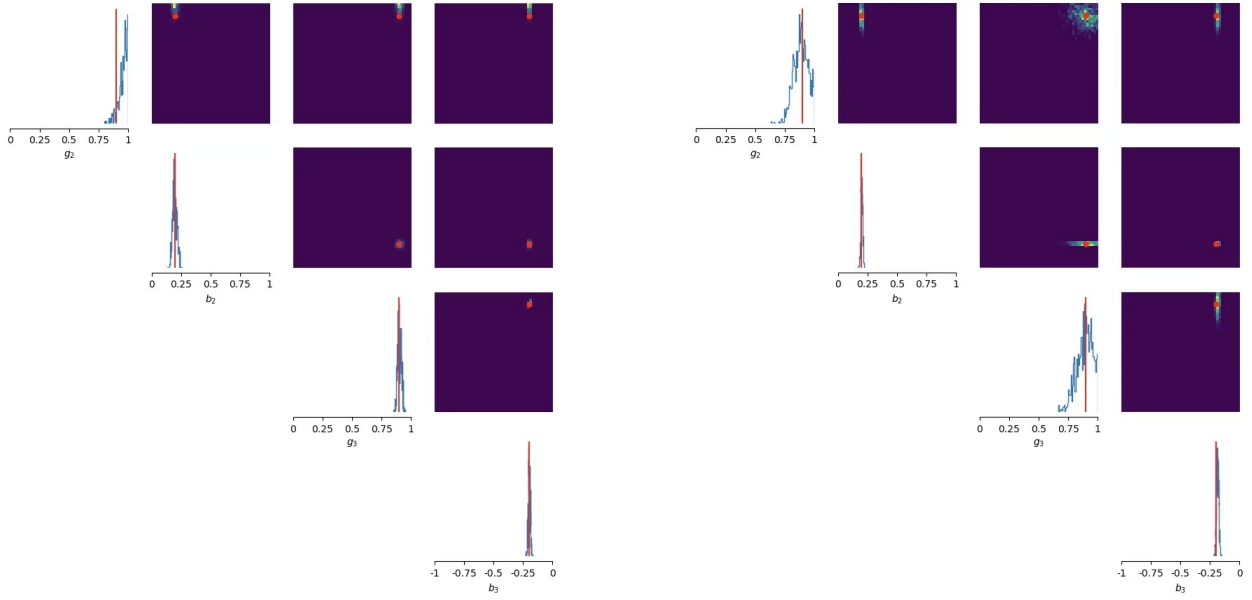


Figure 1: Ground truth posterior distribution under different  $\beta$  values

### 3.2 The approximate ground-truth posterior

By rewriting the system in Equation (2) and (3) defining the Brock–Hommes model, we are able to express the transition density for the observation  $y_{t+1}$  as

$$p(y_{t+1} | y_{1:t}, \theta) = \mathcal{N}\left(y_{t+1}; f(y_{t-2:t}; \theta), \frac{\sigma^2}{R^2}\right), \quad (8)$$

with

$$f(y_{t-2:t}; \theta) = \frac{1}{R} \sum_{h=1}^H \frac{\exp\{\beta(y_t - Ry_{t-1})(g_h y_{t-2} + b_h - Ry_{t-1})\}}{\sum_{h'=1}^H \exp\{\beta(y_t - Ry_{t-1})(g_{h'} y_{t-2} + b_{h'} - Ry_{t-1})\}} (g_h y_t + b_h). \quad (9)$$

Using this expression, we can evaluate the model's likelihood function numerically and obtain samples from an approximations of ground-truth posterior distribution under different  $\beta$  values via Metropolis–Hastings (MH) as shown in Figure 1.

### 3.3 The Effect of the Intensity Parameter on the Posterior Distribution

In the Brock–Hommes model, the intensity of choice  $\beta > 0$  governs how sensitively agents switch between forecasting strategies. The structural parameters  $\theta = (g_2, b_2, g_3, b_3)$  determine the forecasting rules for two representative types. Rewriting Equation (2), the fraction of agents adopting strategy  $h$  is given by

$$n_{h,t}(\beta, \theta) = \frac{\exp(\beta U_{h,t}(\theta))}{\sum_k \exp(\beta U_{k,t}(\theta))}, \quad (10)$$

where  $U_{h,t}(\theta) = (x_t - Rx_{t-1})(g_h x_{t-2} + b_h - Rx_{t-1})$  denotes the past performance of the corresponding strategies.

As  $\beta \rightarrow 0$ , the strategy fractions satisfy

$$n_{h,t}(\beta, \theta) = \frac{1}{H},$$

implying that the system behaves in an almost linear and weakly responsive manner. In this regime the Jacobian norm  $\|\partial x / \partial \theta\|$  becomes small, the likelihood surface is nearly flat. Consequently, the posterior becomes weakly concentrated around the true parameter values, displays strong parameter correlations arising from the effective collinearity of forecasting rules, and is heavily influenced by the prior distribution.

For moderate  $\beta$  values, the model generates clear nonlinear features such as volatility clustering, amplification of deviations, and persistent departures from fundamental values. In this region the sensitivity  $\|\partial x / \partial \theta\|$  reaches its maximal statistical magnitude, yielding a likelihood that is locally well-approximated by a quadratic expansion around the true parameter vector  $\theta^*$ . The resulting posterior distribution is sharply concentrated, exhibits narrow credible regions, and displays a parameter correlation structure that is both stable and interpretable.

When  $\beta$  becomes extremely large, the discrete choice rule approaches a discontinuous mapping,

$$n_{h,t}(\beta, \theta) \approx \begin{cases} 1, & U_{h,t} = \max_k U_{k,t}, \\ 0, & \text{otherwise,} \end{cases}$$

which pushes the price dynamics into a chaotic situation. In this case the trajectory becomes extremely sensitive to small changes in  $\theta$ , while the statistical properties of the simulated series may remain similar across wide regions of the parameter space. As a result, the likelihood surface can develop very steep local curvature in certain directions while simultaneously exhibiting global irregularity or multimodality. The posterior distribution may therefore deviate substantially from Gaussianity and may even split into multiple separated structures.

Considering the situation where a model is pre-trained under  $\beta_0$  (e.g.  $\beta_0 = 120$ ) but the observed data are generated under a different value  $\beta_1$  (e.g.  $\beta_1 = 60$ ). Because the likelihoods

$$L_{\beta_0}(y | \theta) \quad \text{and} \quad L_{\beta_1}(y | \theta)$$

induce different curvature structures in parameter space, one has

$$\nabla_{\theta} \log L_{\beta_0}(y_{\beta_1} | \theta) \neq \nabla_{\theta} \log L_{\beta_1}(y_{\beta_1} | \theta).$$

In summary, the intensity parameter  $\beta$  determines the degree of nonlinearity in the Brock–Hommes model and thereby regulates the Fisher information content embedded in the data. Small values of  $\beta$  produce weak identifiability and diffuse posteriors, intermediate values generate maximal information and sharply concentrated distributions, and large values may induce quasi-chaotic dynamics that result in irregular or multimodal posteriors. As a consequence, transferring a model trained under one value of  $\beta$  to data generated under another can naturally produce structural biases in the inferred parameters, particularly those governing level-adjustment mechanisms such as  $b_2$ .

## 4 Test-Time Training of Deep Neural Networks for ABM

As discussed in Section 3.3, the posterior distributions under two  $\beta$  values have different shapes, and a neural network trained at  $\beta=120$  does not have the ability to directly generalize to  $\beta=60$ . Based on the slight effect of  $\beta$  on the posterior distributions of the parameters, we want to adjust a pre-trained model which is based on the Brock-Hommes model with  $\beta=120$ , to a setting where the Brock-Hommes model with  $\beta=60$ .

To solve this distribution shift, we take the neural network when making the estimation of the posterior distribution of the parameters trained at  $\beta=120$  as initialization and fine-tune it using simulations generated at  $\beta=60$ . This allows the model to retain the structural information learned from the high- $\beta$  model while adjusting its network parameters to match the lower- $\beta$  posterior feature. Two typical strategies have been combined with Sequential Neural Posterior Estimation to achieve fine-tuning goal in this section, Full Parameter Test-Time Training (SNPE-TTT) and Low-Rank Adaptation (SNPE-LoRA). As a result, the fine-tuned model can accurately approximate the posterior for  $\beta=60$  without training the whole deep learning network from the beginning. This enables rapid adaptation to new tasks with limited data by combining the knowledge embedded in a pretrained model, resulting in more stable and accurate performance.

### 4.1 Full Parameter Test-Time Training with SNPE (SNPE-TTT)

The weight parameters of neural networks trained under the environment of Brock-Hommes Model with  $\beta = 120$  have obtained significant information about this specific ABM, although it is not able to directly adjust to this ABM with different  $\beta$  values. This pre-learned information allows fast adjustments of the neural network for new observations without retraining.

To adapt to the lower  $\beta$  value of Brock-Hommes model with noisy observations, we apply Full Parameter Test-Time Training based on SNPE. This procedure updates all learnable weights of the pre-trained network. Starting from a well-informed initialization, the network is exposed to generated under the target  $\beta$  value, and each SNPE round improves the posterior by incorporating these additional simulations and optimizing the entire weight parameter set. This ensures that the estimator can fully realign its learned feature representations and likelihood structure. As a result, full fine-tuning achieves faster convergence, higher posterior accuracy, and improved robustness to distributional shifts.

## 4.2 Low-Rank Adaptation with SNPE (SNPE-LoRA)

In contrast to SNPE-TTT, we also apply the Low-Rank Adaptation combined with SNPE (SNPE-LoRA) strategy, which injects trainable low-dimensional matrices into specific weight layers while keeping the original pre-trained parameters frozen. For the original pre-trained weight matrix  $W_0 \in \mathbb{R}^{d \times k}$ , LoRA updates the weight parameter in low-rank form as

$$W' = W_0 + \Delta W, \quad \Delta W = BA, \quad (11)$$

where  $A \in \mathbb{R}^{r \times k}$  and  $B \in \mathbb{R}^{d \times r}$  with  $r \ll \min(d, k)$ . Only the matrices  $A$  and  $B$  are optimized during fine-tuning, whereas the original weight  $W_0$  remains fixed. In practice, SNPE-LoRA initializes the adapter matrices  $A$  and  $B$  in the Equation (7) as the following

$$A \sim \mathcal{N}(0, \sigma^2), \quad B = 0.$$

This choice ensures that the initial update is exactly zero,

$$\Delta W = BA = 0,$$

and therefore the weight parameters of neural network remain the same as the pretrained parameter  $W_0$  at the beginning of SNPE-LoRA. This guarantees that SNPE-LoRA does preserve the behaviour of the pretrained model before gradient updates.

Within the SNPE framework, LoRA modules are inserted into the density estimator so that each inference round updates only the low-rank but significant components. This allows rapid adaptation while preserving the most important information embedded in the pre-trained model. Due to its parameter efficiency, SNPE-LoRA yields faster training, lower memory consumption, and reduced overfitting risk, although its restricted update subspace may limit expressiveness when the target model differs substantially from the pre-trained environment.

---

**Algorithm 2** SNPE-LoRA

---

**Input:** Prior distribution  $p(\theta)$ , simulator  $p_{\beta_1}(x | \theta)$ , observation  $y$ , SNPE-LoRA rank  $r$ , number of fine-tuning rounds  $M$ , simulations per round  $N$ .

Freeze all pretrained parameters  $\phi^{(0)}$ .

Insert LoRA modules on selected layers:

$$\Delta W = AB, \quad A \in \mathbb{R}^{d \times r}, \quad B \in \mathbb{R}^{r \times d},$$

with  $A, B$  trainable and initialized randomly.

Initialize proposal distribution:

$$\tilde{p}_0(\theta) = p(\theta)$$

Initialize dataset  $\mathcal{D} = \{\}$ .

**for**  $m = 0, \dots, M - 1$  **do**

    Sample parameters:

$$\theta_n^{(m)} \sim \tilde{p}_m(\theta), \quad n = 1, \dots, N$$

    Simulate data:

$$x_n^{(m)} \sim p_{new}(x | \theta_n^{(m)}).$$

    Append dataset:

$$\mathcal{D} := \mathcal{D} \cup \bigcup_{n=1}^N \{(x_n^{(m)}, \theta_n^{(m)})\}.$$

**LoRA fine-tuning step**

**while** not converged **do**

    Compute SNPE loss:

$$\mathcal{L}(\phi^{(0)}, A, B) = - \sum_{(x, \theta) \in \mathcal{D}} \log \left( q_{\phi^{(0)} + \Delta W}(\theta | x) \frac{\tilde{p}_m(\theta)}{p(\theta)} \frac{1}{Z(x)} \right)$$

    Update only LoRA parameters:

$$A \leftarrow A - \eta \nabla_A \mathcal{L}, \quad B \leftarrow B - \eta \nabla_B \mathcal{L}.$$

**end while**

    Update proposal distribution:

$$\tilde{p}_{m+1}(\theta) = q_{\phi^{(0)} + AB}(\theta | y).$$

**end for**

**Output:** SNPE-LoRA fine-tuned posterior estimator  $q_{\phi^{(0)} + AB}(\theta | y)$ .

---

## 5 Initial Numerical Experiments for Test-Time Training

We generate two synthetic datasets using the Brock-Hommes model under  $\beta = 120$  and  $\beta = 60$ . The two datasets correspond to `bh_beta120` and `bh_beta60`. In our setting, these two models only differs in the choice of  $\beta$  values, their internal configurations, including the ground-truth value of the parameters  $\theta^*$  and the associated prior distributions are the same. In other words, for the two

scenarios, both the true parameter values and the parameter priors are specified to be manually aligned, so that we can ensure that the only source of distributional shift comes exclusively from the change in the intensity parameter  $\beta$ . By keeping all structural and parametric components identical, we isolate the effect of  $\beta$  on the data-generating process and eliminate confounding factors arising from differences in the underlying parameter space. This controlled design enables a clean evaluation of how well the original model trained under  $\beta = 120$  can adapt to a new  $\beta = 60$  regime purely through test-time training, without interference from changes in the ground truth parameters or the prior specification.

In addition, we conduct a second  $\beta = 60$  experiment, denoted by `bh_beta60gtc`, in which we intentionally introduce a mismatch in the ground-truth parameters while keeping the prior specification unchanged. Concretely, we generate another dataset under  $\beta = 60$  but set the ground-truth value to a different configuration  $\tilde{\theta}^*$ . Unlike the aligned `bh_beta60` setting, this experiment simultaneously induces a shift in the data-generating mechanism through both the intensity parameter  $\beta$  and the location of the true parameters in the parameter space. This additional setting allows us to assess fine-tuning robustness under a more challenging form of distributional shift, where adaptation cannot be attributed solely to  $\beta$ -variation but must also accommodate a change in the underlying ground truth.

Let

$$\begin{aligned}\theta^* &= (g_{2,s}^*, b_{2,s}^*, g_{3,s}^*, b_{3,s}^*) = (0.9, 0.2, 0.9, -0.2), \\ \tilde{\theta}^* &= (\tilde{g}_{2,s}^*, \tilde{b}_{2,s}^*, \tilde{g}_{3,s}^*, \tilde{b}_{3,s}^*) = (0.6, 0.4, 0.7, -0.3), \\ g_2 &\sim \mathcal{U}(0, 1), \quad b_2 \sim \mathcal{U}(0, 1), \quad g_3 \sim \mathcal{U}(0, 1), \quad b_3 \sim \mathcal{U}(-1, 0).\end{aligned}$$

denote the ground-truth values (for `bh_beta120/bh_beta60` and `bh_beta60gtc`, respectively) and the shared prior distributions for the four parameters.

**Hyperparameter of SNPE-TTT and SNPE-LoRA** To adapt the pre-trained Brock-Hommes model under  $\beta = 120$  to the new tasks, we employ full parameter SNPE-TTT training schedule. The number of simulations in each round is given by [500, 500, 500, 1000], corresponding to four sequential rounds of simulation-based inference.

For SNPE-LoRA, we set all hyperparameter the same as Full Fine-Tuning in order to control numerical experiment variables, so that we can exclude the influence of these model structural parameters. Additionally, we apply the LoRA scaling rule

$$\Delta W_{\text{scaled}} = \frac{\alpha}{r} BA.$$

In all experiments we set:

$$\begin{aligned}r &= \text{LORA\_RANK} = 8, \\ \alpha &= \text{LORA\_ALPHA} = 8.\end{aligned}$$

## 5.1 Performance Metrics

To quantify the discrepancy between the estimated posterior  $\hat{\pi}(\theta | x)$  and the ground truth posterior  $\pi^*(\theta | x)$ , we adopt the two integral probability metrics.

**Wasserstein Distance (WASS).** Let  $\{\theta_i\}_{i=1}^B \sim \pi^*$  and  $\{\tilde{\theta}_j\}_{j=1}^Z \sim \hat{\pi}$ . The Wasserstein distance is

$$W(\pi^*, \hat{\pi}) = \inf_{\gamma \in \Gamma_{B,Z}} \sum_{i=1}^B \sum_{j=1}^Z \|\theta_i - \tilde{\theta}_j\|_2 \gamma_{ij},$$

where  $\Gamma_{B,Z}$  is the set of non-negative transport matrices  $B \times Z$  with row sums  $Z^{-1}$  and column sums  $B^{-1}$ . The smaller  $W$  indicates stronger agreement between the distributions.

**Maximum Mean Discrepancy (MMD).** Let  $k(\cdot, \cdot)$  be a positive semi-definite kernel. The squared MMD is

$$\text{MMD}^2(\pi^*, \hat{\pi}) = \mathbb{E}_{\theta, \theta' \sim \pi^*}[k(\theta, \theta')] + \mathbb{E}_{\tilde{\theta}, \tilde{\theta}' \sim \hat{\pi}}[k(\tilde{\theta}, \tilde{\theta}')] - 2 \mathbb{E}_{\theta \sim \pi^*, \tilde{\theta} \sim \hat{\pi}}[k(\theta, \tilde{\theta})].$$

We use an RBF kernel

$$k(\theta, \tilde{\theta}) = \exp\left(-\frac{\|\theta - \tilde{\theta}\|_2^2}{2\eta^2}\right),$$

where the bandwidth  $\eta^2$  is set via the median heuristic. Lower MMD indicates better posterior inference.

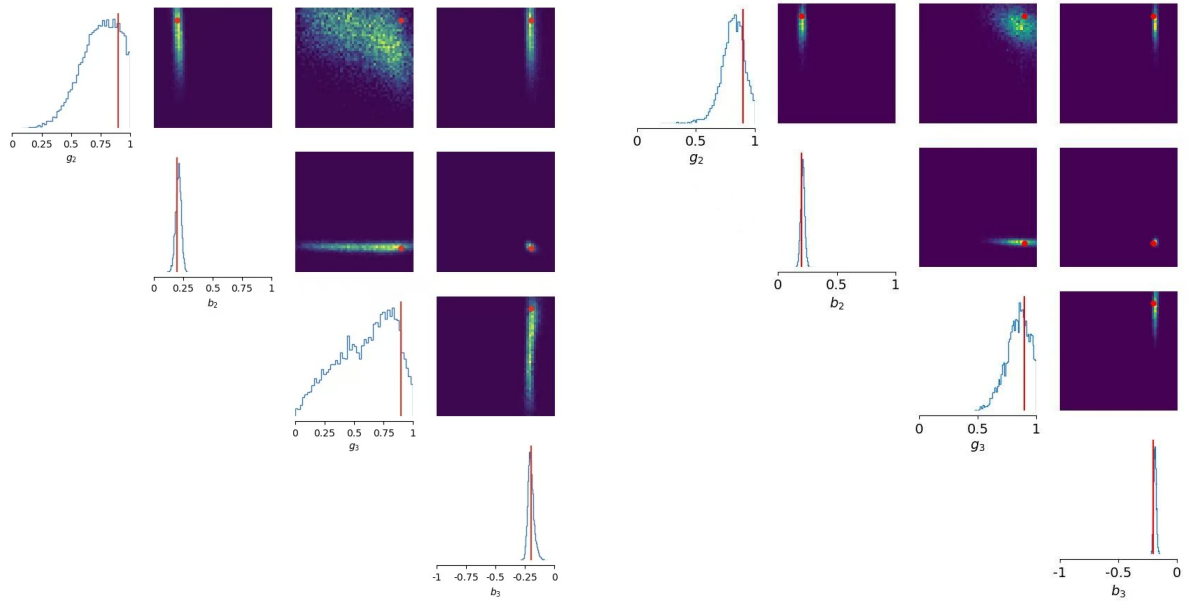
Both metrics are calculated between posterior samples from our estimator  $\hat{\pi}$  and the approximate of ground truth posterior samples obtained by Metropolis–Hastings as described in Section 2.1.2.

## 5.2 Posterior Comparison

Figure 2 and Figure 3 compare the posterior samples obtained by SNPE, SNPE-TTT, and SNPE-LoRA with the ground truth posterior distributions resulted from two experiments, respectively, which characterizes the intrinsic uncertainty of the parameters under the data-generating process and serves as a more informative target for evaluating posterior calibration.

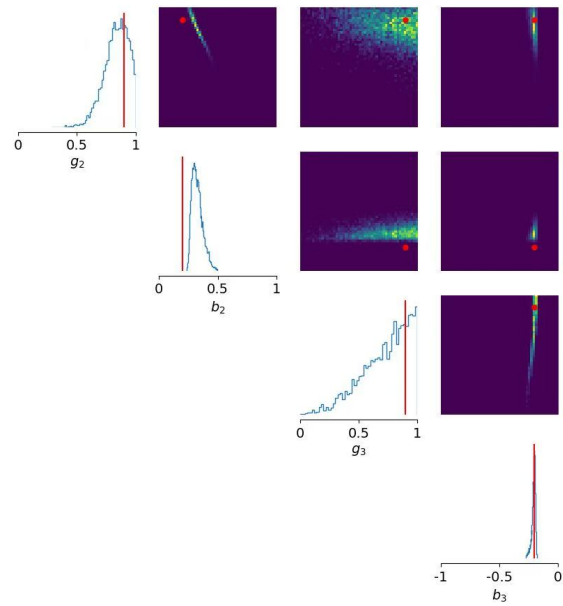
In the context of `bh_beta60` shown in Figure 2, across the parameters  $\theta = (g_2, b_2, g_3, b_3)$ , the posterior inference generated by SNPE-TTT aligns the most closely with the shape, location, and spread of the ground-truth distributions. In particular, the marginal densities of  $g_2$  and  $g_3$  match the ground-truth modes and reproduce the correct degree of skewness. For  $b_2$  and  $b_3$ , the fine-tuned posterior captures the narrow variance, indicating successful adaptation to the new model with different  $\beta$  value. SNPE-LoRA achieves partial correction relative to SNPE but remains constrained by the low-rank update. Although it can change the shape of posterior distribution toward the ground-truth distribution under  $\beta = 60$ , it underestimates the curvature of the joint structure and occasionally exhibits residual bias, most visibly in the  $b_2$ . This highlights the expressiveness limitation of low-rank adaptation when the target model differs substantially from the pre-training model.

In the `bh_beta60gtc` setting shown in Figure 3, where the ground-truth parameters are shifted, all three methods produce noticeably more concentrated posteriors, and the discrepancy becomes more dominated by subtle changes in location and dependence structure rather than large-scale mode mismatch. SNPE already yields a relatively well-calibrated posterior around the shifted ground-truth values, with marginal peaks close to the truth and compact joint density regions, indicating that part of the shift can be absorbed by the pretrained representation even without explicit adaptation. SNPE-TTT further sharpens the marginals and aligns the posterior mass tightly around the ground-truth point across all four coordinates, leading to the most consistent recovery of the correct location and spread. SNPE-LoRA remains capable of matching the dominant mode in this regime, but it still shows residual mismatch in the joint geometry, where the learned dependence can become overly restrictive or slightly distorted, which is most visible in the coupling patterns involving  $b_2$ . Overall, Figure 3 suggests that when the distributional shift is driven jointly by  $\beta$  and a change in  $\theta^*$ , low-rank adaptation may correct the main location of the posterior while being less reliable in reproducing the full joint structure.



(a) SNPE

(b) SNPE-TTT (Full Fine-Tuning)



(c) LoRA-SNPE

Figure 2: Posterior Comparison Between SNPE, SNPE-TTT and SNPE-LoRA under `bh_beta60`

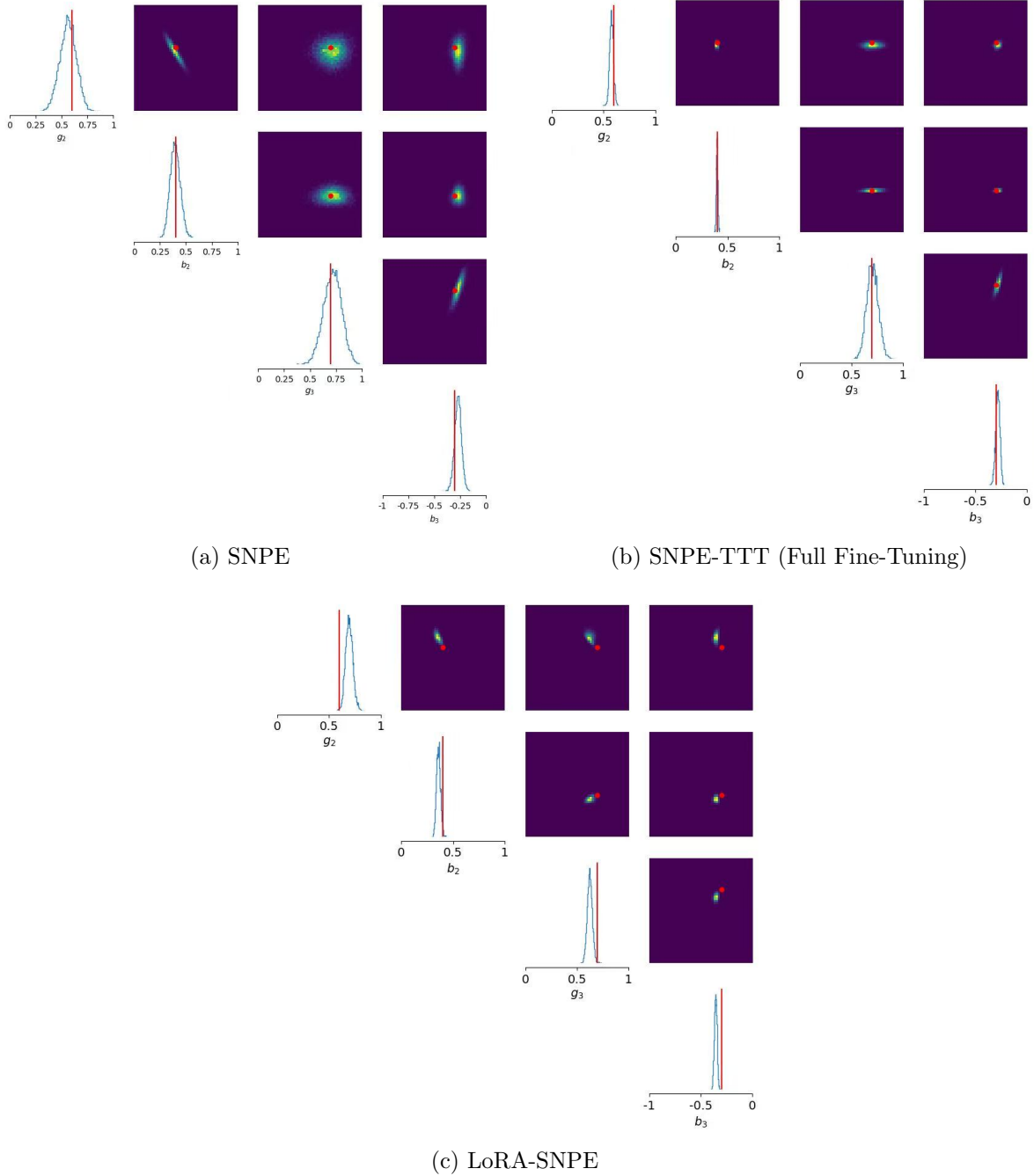


Figure 3: Posterior Comparison Between SNPE, SNPE-TTT and SNPE-LoRA under `bh_beta60gtc`

### 5.3 Discrepancy Comparison

Table 1 reports the discrepancies between the estimated posteriors and the ground-truth distribution, measured by the Wasserstein (WASS) distance and the Maximum Mean Discrepancy (MMD). The results reveal distinct performance patterns across the three methods under the two  $\beta = 60$  settings (`bh_beta60` and `bh_beta60gtc`).

For `bh_beta60`, SNPE exhibits the largest divergence from the reference posterior, with both WASS (0.3272) and MMD (0.1777) substantially higher than those of the two test-time training

approaches. SNPE-TTT achieves the best overall performance, reducing WASS to 0.1551 and MMD to 0.0451. This confirms that updating all pretrained weights allows the density estimator to fully adapt its feature representation and likelihood to the new model, yielding the closest match to the ground-truth posterior. SNPE-LoRA performs consistently better than SNPE but remains higher discrepancy than full fine-tuning, with intermediate WASS (0.2144) and MMD (0.0813) values. Among all methods, SNPE-TTT yields the most reliable correction, achieving the smallest discrepancies under both metrics. SNPE-LoRA also outperforms the unadapted SNPE baseline while updating far fewer parameters; however, its low-rank constraint can limit the expressivity of the adaptation, leaving systematic residual mismatch in the joint dependence structure and tail behaviour, and therefore producing intermediate discrepancy values.

For `bh_beta60gtc`, where the ground-truth parameters are additionally shifted, SNPE attains relatively small discrepancies in this setting with WASS (0.0888), MMD (0.0024), while SNPE-TTT still yields the smallest WASS (0.1693) and the lowest MMD (0.0014). However, SNPE-LoRA incurs the largest WASS (0.0355) and MMD (0.0562). SNPE-TTT attains the lowest discrepancy under both metrics, whereas SNPE-LoRA yields substantially larger discrepancy, suggesting not only limited gains but an overall degradation relative to the unadapted baseline. A plausible interpretation is that low-rank updates can sometimes account for coarse, transport-level adjustments, such as dominant location or scale shifts or a few principal directions of variation, but may fail when successful adaptation requires coordinated changes to the conditional geometry of the flow, including higher-order dependencies, tail behavior, multi-modality, and local curvature. In particular, the SNPE-LoRA restricts parameter updates to a low-dimensional subspace, which can systematically underfit directions that are essential for matching conditional correlations and coupling interactions, and thus inducing anisotropic or uneven correction across layers. Under limited test-time data, this restricted parametrization may further bias optimization toward a small set of dominant update directions, so the model compensates by over-adjusting within the representable subspace, thereby amplifying mismatch in unrepresented directions and leading to consistently larger discrepancies. Therefore, existing parameter-efficient approach is not stable in posterior estimation of ABMs.

Task	Method	WASS	MMD
bh_beta60	SNPE	0.3272	0.1777
	SNPE-TTT	0.1551	0.0451
	SNPE-LoRA	0.2144	0.0813
bh_beta60gtc	SNPE	0.0888	0.0024
	SNPE-TTT	0.0355	0.0014
	SNPE-LoRA	0.1693	0.0562

Table 1: Discrepancies between the approximate ground-truth posterior and the posteriors estimated with SNPE and different Fine-tuning methods under two metrics.

## 6 Gradient-Subspace Test-Time Training and Parameter-Efficient Adaptation

As shown in the previous sections, a posterior estimator produced by classical test-time training, which updates a pre-trained network at deployment time using only target-domain data, can become systematically miscalibrated when encountered distribution shift. In ABMs settings, we can exploit the simulator to generate a small labeled target dataset and directly minimize the SNPE objective

at test time. However, full-parameter SNPE-TTT scales with the full network dimension and can become computationally expensive. Parameter-efficient fine-tuning (PEFT) methods such as LoRA constrain updates in weight space via low-rank reparameterizations, but may underfit when adaptation requires loss-specific, coordinated changes in the conditional dependence structure of a normalizing-flow posterior.

To address this trade-off, we propose an *objective-directed* approach extending the gradient-subspace fine-tuning approaches [3, 15, 10] to our SNPE setting: learning a low-dimensional *adaptation subspace* from *target gradients* around the pre-trained parameters and then restrict subsequent optimization to this subspace. We introduce two variants: **GradSubspace-TTT**, which projects test-time gradients onto the learned subspace via backward hooks; and **GradSubspace-PEA**, which reparameterizes adaptation explicitly in the subspace and optimizes only the low-dimensional coefficients.

Let  $q_\phi(\theta | x)$  denote the amortised SNPE posterior network (a conditional normalizing flow) with parameters  $\phi \in \mathbb{R}^d$ . Given a small target dataset  $\mathcal{D}_{\text{new}} = \{(\theta_i, x_i)\}_{i=1}^{N_{\text{new}}}$  generated under the shifted simulator, gradient-based test-time training optimizes the same objective used during SNPE training, SNPE-TTT and SNPE-LoRA.

## 6.1 Stage I: learning a gradient adaptation subspace.

Let  $\phi_0$  denote the pre-trained parameters, flattened over the subset of weights allowed to adapt at test time. We split a small portion of  $\mathcal{D}_{\text{new}}$  into  $B$  mini-batches  $\{\mathcal{B}_1, \dots, \mathcal{B}_B\}$ . Mini-batching produces multiple stochastic gradient probes of the target loss landscape while keeping the snapshot cost low. For each batch  $\mathcal{B}_b$ , similar to [3], we compute a gradient snapshot at  $\phi_0$ :

$$g_b = \nabla_\phi \mathcal{L}(\phi_0; \mathcal{B}_b) \in \mathbb{R}^d, \quad b = 1, \dots, B, \quad (12)$$

and stack them into the snapshot matrix  $G = [g_1, \dots, g_B] \in \mathbb{R}^{d \times B}$ . Then, we conduct the Singular Value Decomposition to the gradient snapshot matrix  $G = U \Sigma V^\top$ , with a rank  $r \leq B$ . Specifically, a strategy to choose  $r$  is using energy criterion  $\sum_{i \leq r} \sigma_i^2 / \sum_{i \leq B} \sigma_i^2 \geq \tau$ , so that we can obtain the smallest  $r$  satisfying above condition. Following  $U_r \in \mathbb{R}^{d \times r}$  is retained and then defines the *gradient adaptation subspace*

$$\mathcal{S} = \text{span}(U_r),$$

with the orthogonal projector

$$\Pi = U_r U_r^\top, \quad \Pi(g) = U_r (U_r^\top g), \quad (13)$$

which can be applied in  $O(dr)$  time per gradient after Stage I. Intuitively,  $\mathcal{S}$  captures the dominant directions along which the target objective decreases locally around  $\phi_0$ , making it *loss-aware* rather than purely weight-geometry-driven.

## 6.2 Stage II: Subspace-constrained adaptation

After identifying the adaptation subspace based on the loss gradient, we propose two approaches to achieve fine-tuning, *GradSubspace Test-Time Training (GradSubspace-TTT)* and *GradSubspace Parameter Efficient Adaptation (GradSubspace-PEA)*. These two gradient subspace test-time training approaches are presented in Algorithm 3.

**Stage II of GradSubspace-TTT: projected-gradient adaptation via backward hooks.** GradSubspace-TTT constrains test-time optimisation by projecting every backpropagated gradient onto  $\mathcal{S}$ . For an adaptation iterate  $\phi_t$  and batch  $\mathcal{B}_t$ , we compute  $g_t = \nabla_\phi \mathcal{L}(\phi_t; \mathcal{B}_t)$  and replace it by its projection

$$\tilde{g}_t = \Pi(g_t) = U_r(U_r^\top g_t), \quad (14)$$

then update using any first-order optimizer driven by  $\tilde{g}_t$ :

$$\phi_{t+1} \leftarrow \phi_t - \eta \tilde{g}_t. \quad (15)$$

We implement (14) efficiently via backward hooks on the chosen parameter blocks, so both updates and optimiser states evolve only in the low-dimensional subspace  $\mathcal{S}$ . From an optimization viewpoint, this is closely related to subspace-constrained first-order schemes; projected gradient descent in nonconvex low-dimensional parameterizations has been analyzed in related contexts.

**Stage II of GradSubspace-PEA: reparameterized subspace optimization.** While the first GradSubspace-TTT constrains the *update direction*, it still optimises  $\phi \in \mathbb{R}^d$  and maintains optimizer state in the full parameter space. GradSubspace-PEA achieves *parameter efficiency* by explicitly restricting adaptation to the affine subspace  $\phi_0 + \text{span}(U_r)$ :

$$\phi(c) = \phi_0 + U_r c, \quad c \in \mathbb{R}^r, \quad (16)$$

and optimizing only the coefficient vector  $c$ :

$$\min_{c \in \mathbb{R}^r} \mathcal{L}(\phi_0 + U_r c; \mathcal{D}_{\text{new}}). \quad (17)$$

By the chain rule, for any mini-batch  $\mathcal{B}$ ,

$$\nabla_c \mathcal{L}(\phi_0 + U_r c; \mathcal{B}) = U_r^\top \nabla_\phi \mathcal{L}(\phi_0 + U_r c; \mathcal{B}), \quad (18)$$

so the trainable dimension and optimizer state reduce from  $d$  to  $r$ , while the subspace constraint is enforced exactly by construction.

---

**Algorithm 3** SNPE with GradSubspace Adaptation

---

**Input:** Prior  $p(\theta)$ , simulator  $p_{\beta_1}(x \mid \theta)$ , observation  $y$ , pretrained parameters  $\phi^{(0)}$ , method flag MODE  $\in \{\text{TTT, PEA}\}$ , rounds  $M$ , sims/round  $N$ , snapshot batches  $B$ , rank  $r$  (or energy threshold  $\tau$ ), step size  $\eta$ , optimizer Optim.

**Result:** Adapted posterior estimator  $q_{\phi^*}(\theta \mid y)$ .

Set proposal  $\tilde{p}_0(\theta) = p(\theta)$ , dataset  $\mathcal{D} = \emptyset$ .

Set current parameters  $\phi \leftarrow \phi^{(0)}$ .

**for**  $m = 0, \dots, M - 1$  **do**

    Sample  $\theta_n^{(m)} \sim \tilde{p}_m(\theta)$ ,  $n = 1, \dots, N$ .

    Simulate  $x_n^{(m)} \sim p_{\beta_1}(x \mid \theta_n^{(m)})$ ,  $n = 1, \dots, N$ .

    Append dataset  $\mathcal{D} \leftarrow \mathcal{D} \cup \{(x_n^{(m)}, \theta_n^{(m)})\}_{n=1}^N$ .

    Define SNPE round loss on any set  $\mathcal{S}$ :

$$\mathcal{L}_m(\phi; \mathcal{S}) = - \sum_{(x, \theta) \in \mathcal{S}} \log \left( q_{\phi}(\theta \mid x) \frac{\tilde{p}_m(\theta)}{p(\theta)} \frac{1}{Z(x)} \right).$$

**Subspace identification at round  $m$  (using  $\phi^{(0)}$ )**

Split (a subset of)  $\mathcal{D}$  into  $B$  mini-batches  $\{\mathcal{B}_1, \dots, \mathcal{B}_B\}$ .

**for**  $b = 1, \dots, B$  **do**

    Compute gradient snapshot:

$$g_b \leftarrow \nabla_{\phi} \mathcal{L}_m(\phi^{(0)}; \mathcal{B}_b),$$

**end for**

Form snapshot matrix  $G \leftarrow [g_1, \dots, g_B]$ , compute SVD  $G = U \Sigma V^{\top}$  and choose  $r$ .

Set  $\Pi(g) = U_r(U_r^{\top} g)$

**if** GRADSUBSPACE-TTT **then**

    Register a backward hook that maps each gradient tensor  $g$  to  $\Pi(g)$  on blocks.

**while** not converged **do**

        Evaluate loss  $\ell \leftarrow \mathcal{L}_m(\phi; \mathcal{D})$ .

        Backpropagate and apply the hook to obtain projected gradients.

        Update  $\phi \leftarrow \text{Optim}(\phi; \eta)$ .

**end while**

**end if**

**if** GRADSUBSPACE-PEA **then**

    Freeze base parameters  $\phi^{(0)}$  and define  $\phi(c) = \phi^{(0)} + U_r c$ , with  $c \in \mathbb{R}^r$ .

    Initialise  $c \leftarrow 0$ .

**while** not converged **do**

        Evaluate loss  $\ell \leftarrow \mathcal{L}_m(\phi^{(0)} + U_r c; \mathcal{D})$ .

        Compute  $\nabla_c \ell = U_r^{\top} \nabla_{\phi} \mathcal{L}_m(\phi^{(0)} + U_r c; \mathcal{D})$ .

        Update  $c \leftarrow \text{Optim}(c; \eta)$ .

**end while**

    Set  $\phi \leftarrow \phi^{(0)} + U_r c$ .

**end if**

    Update proposal  $\tilde{p}_{m+1}(\theta) = q_{\phi}(\theta \mid y)$ .

**end for**

**Output:**  $q_{\phi}(\theta \mid y)$ .

---

## 7 Numerical Experiments for GradSubspace Test-Time Training

To keep the consistence with numerical experiments of SNPE-TTT and SNPE-LoRA in Section 5, we conduct the same experiments to evaluate the Gradient-Subsapce test-time training approaches, from `bh_beta120` to `bh_beta60` and `bh_beta60gtc`. Additionally, the hyperparameters are also kept the same with SNPE-TTT and SNPE-LoRA. We take [500, 500, 500, 1000] as the number of simulations at each round of simulation-based SNPE, and  $r = 8$  as the rank of singular value decomposition of gradient snapshot matrix.

### 7.1 Posterior Comparison

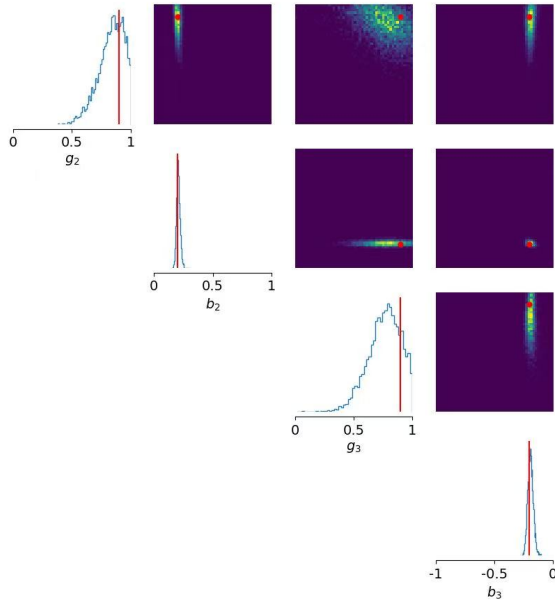
Figure 4 compares the posterior samples produced by GradSubspace-TTT and GradSubspace-PEA under the context of `bh_beta60` and `bh_beta60gtc`. Each subfigure presents the marginal densities on the diagonal and pairwise joint densities. The same as Figure 2 and Figure 3, the marginal plot in Figure 4 also includes a vertical red line that marks the ground-truth value of the parameters used for visual calibration. The most significant observation is that GradSubspace-TTT and GradSubspace-PEA output nearly identical posterior shapes in both setting. This agreement suggests that the learned gradient subspace is the main factor that drives posterior correction, while the two parameterizations provide different implementation and memory trade-offs without changing the inferred posterior geometry in a visible way.

Specifically, in the `bh_beta60` setting as shown in Figure 4a and Figure 4c, both GradSubspace variants produce concentrated marginals shapes for  $b_2$  and  $b_3$ , and the corresponding joint density regions remain compact. These two methods also successfully reproduce the wider property of posterior distribution in the estimation of  $g_2$  and  $g_3$ , which is aligned with the ground-truth distribution of two parameters. This behavior is consistent with the discussion in Section 3.3, where  $\beta$  controls the information content and local curvature of the likelihood. In particular, when  $\beta$  decreases, the effective sensitivity of the trajectory to  $\theta$  weakens in certain directions, which leads to a wider posterior of  $g_2$  and  $g_3$ . Therefore, it indicates that two gradient-based test-time training approaches, GradSubspace-TTT and GradSubspace-PEA captured key information to adapt the network fitting into the distribution shift and initially shows that they had better performance in posterior estimation in ABMs.

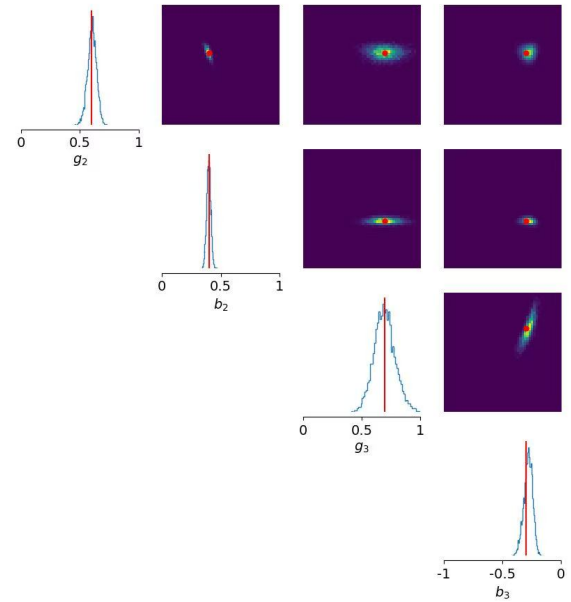
Additionally, in the setting of `bh_beta60gtc`, where the shift is compounded by both  $\beta$  and a changed ground-truth parameter, Figure 4b and Figure 4d show that the posteriors become more concentrated across all four parameters than the distribution conducted by SNPE-TTT and SNPE-LoRA. The diagonal marginals sharpen, and the off-diagonal plots show clean and compact density shapes with clear dependence structure. This behavior is significant since inference quality in SBI is not only about matching marginal peaks, and also about reproducing sharp distribution geometries which are the same as the ground-truth.

These observations also explain that GradSupspace-TTT and GradSubspace-PEA help address the limitations appeared in SNPE-TTT and SNPE-LoRA. While full SNPE-TTT can provide strong correction, it requires updating the full parameter vector and storing full optimizer at test time. The GradSubspace-PEA variant achieves almost the same posterior distribution shape as GradSubspace-TTT in these plots, while updating only a low-dimensional coefficient vector, which supports it as a more accurate parameter-efficient alternative to test-time training. In addition, SNPE-LoRA can only partially correct the posterior location of some parameter, but remains others mismatch with ground-truth because a fixed low-rank weight update can miss task-specific directions that matter for posterior distribution shift correction. The objective-directed GradSubspace variants select update directions from the target gradients. The resulting joint densities in Figure 4 are stable and

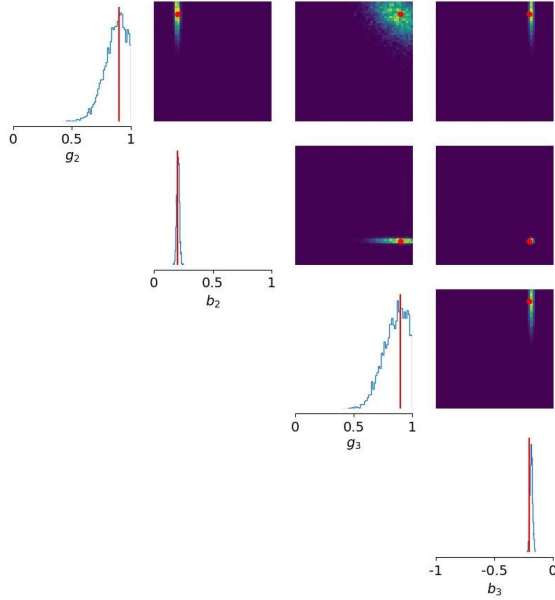
well-shaped, which provides qualitative evidence that gradient-subspace adaptation can reduce the distribution mismatch seen under low-rank adapters while avoiding the full cost of unconstrained test-time training.



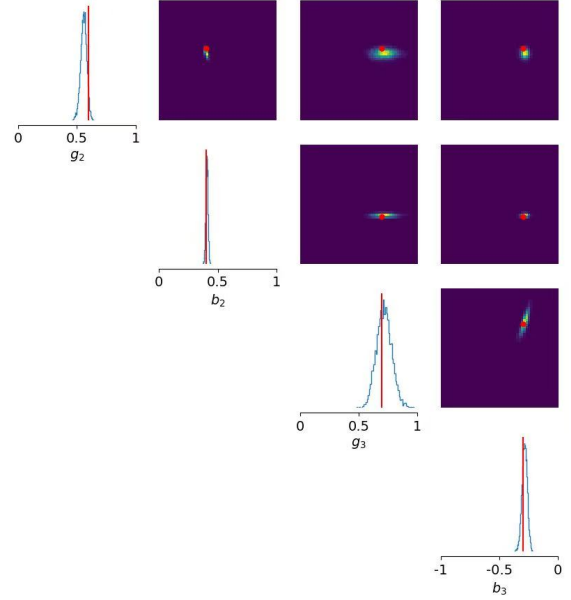
(a) GradSubspaceTTT-SNPE for **beta60**



(b) GradSubspaceTTT-SNPE for **beta60gtc**



(c) GradSubspacePEA-SNPE for **beta60**



(d) GradSubspacePEA-SNPE for **beta60gtc**

Figure 4: Posterior Comparison Between GradSubspace-TTT and GradSubspace-PEA under **beta60** and **beta60gtc**

## 7.2 Discrepancy Comparison

As shown in Table 2, both GradSubspace-TTT and GradSubspace-PEA yield consistently low discrepancies across the two  $\beta = 60$  settings, highlighting the benefit of restricting test-time training to an objective-directed low-dimensional gradient subspace estimated from target batches. For `bh_beta60`, GradSubspace-TTT further improves upon full test-time training, achieving WASS = 0.1408 and MMD = 0.0367. Additionally, GradSubspace-PEA surprisingly attains the lowest discrepancies overall with WASS = 0.0483 and MMD = 0.0043, indicating that in this approach the dominant target-gradient directions capture most of the correction needed to align the learned posterior with the ground-truth distribution. The additional outperformance of GradSubspace-PEA over GradSubspace-TTT is consistent with the interpretation that an explicit low-dimensional reparameterization  $\phi = \phi_0 + U_r c$  reduces gradient noise, thereby producing a more stable posterior correction than projecting gradients into full network weights alone.

In the context of `bh_beta60gtc`, GradSubspace approaches remain robust and continues to reduce discrepancy. GradSubspace-TTT achieves WASS = 0.0676 and MMD = 0.0020, and GradSubspace-PEA further decreases WASS to 0.0497 with a comparable MMD of 0.0021. Importantly, unlike low-rank weight adapters that can deteriorate under stronger distribution shift, the gradient-subspace constraint prevents updates from drifting into poorly supported directions, yielding reliable improvements without sacrificing similarity. Overall, the discrepancy results support the central claim that objective-directed gradient subspaces provide an effective and stable mechanism for test-time posterior correction in SNPE, with particularly strong advantages when the target distribution shift is well-approximated by a small number of dominant gradient directions.

Task	Method	WASS	MMD
<code>bh_beta60</code>	SNPE	0.3272	0.1777
	SNPE-TTT	0.1551	0.0451
	SNPE-LoRA	0.2144	0.0813
	GradSubspace-TTT	0.1408	0.0367
	GradSubspace-PEA	0.0483	0.0043
<code>bh_beta60gtc</code>	SNPE	0.0888	0.0024
	SNPE-TTT	0.0355	0.0014
	SNPE-LoRA	0.1693	0.0562
	GradSubspace-TTT	0.0676	0.0020
	GradSubspace-PEA	0.0497	0.0021

Table 2: Discrepancies between the approximate ground-truth posterior and the posteriors estimated with SNPE, classical Test-Time Training and GradSubspace variants under two metrics.

## 8 Conclusion

Agent-based models (ABMs) have become a workhorse for studying complex economic and social dynamics, however, their practical impact is still limited by reliable parameter inference under changing environments. When the data occurs distribution shift, retraining a flow-based neural posterior estimator is often computational expensive, and using an unadapted amortised posterior can lead to systematic error. This motivates a simple but consequential question: can we adapt a pre-trained normalizing-flow posterior to a specific target task by using only a small amount of target simulation, while keeping adaptation stable and computationally feasible?

We answered this question by introducing test-time training within SNPE(SNPE-TTT) into posterior inference for parameters in ABMs. Rather than using the pre-trained model directly, we view it as a strong initialization that can be fine-tuned. We first evaluated natural and classic SNPE-TTT and SNPE-LoRA. SNPE-TTT provides a straightforward path to adaptation but updates with the full parameter dimension, and SNPE-LoRA reduces learnable parameters by restricting updates to a low-dimensional weight subspace, but it may cause the neural network missing key information during update and therefore becomes infeasible under strong shift.

To address this challenge, we proposed *objective-directed* alternative approaches based on the gradient subspace of the loss function, which identifies a low-dimensional subspace from a few target mini-batches and then restricts subsequent optimization to this subspace. This design is loss-aware so that it is able to capture dominant descent directions of the target objective in a neighborhood of the pre-trained parameters. We implemented two complementary variants. GradSubspace-TTT performs projected-gradient adaptation via backward hooks, while GradSubspace-PEA increase parameter efficiency through an explicit reparameterization  $\phi = \phi_0 + U_r c$  that optimizes only the low-dimensional weights.

Empirically, we conduct numerical experiments to evaluate these test-time training approaches within the Brock–Hommes model, our results provide convergent qualitative and quantitative evidence that our methods can correct flow-based posteriors under distribution shift. In the `bh_beta60` and `bh_beta60gtc` setting, where the shift is driven purely by  $\beta$ , SNPE-TTT substantially reduces discrepancy relative to the SNPE posterior and visibly sharpens posterior mass around the ground truth. However, SNPE-LoRA can degrade markedly, indicating that a fixed low-rank weight may lost directions to fit into new tasks. In contrast, the proposed GradSubspace methods remain robust across both settings and achieve consistently low discrepancies, with posterior geometries that closely track the ground truth in both marginals and joints. Notably, GradSubspace-PEA attains the strongest discrepancy reductions in our study, supporting the interpretation that an explicit low-dimensional reparameterization can reduce gradient noise and improve stability when only limited target data are available.

The broader implication is that where we constrain adaptation matters as much as how much we constrain it. Classic weight-space low-rank adapters trade capacity for efficiency, but they do not explicitly align the restricted subspace with the target inference objective. In contrast, gradient-subspace test-time training update directions that are directly supported by the target loss, thus avoiding drifting into poorly supported parameter directions and improving robustness under complicated shift. This is especially relevant for ABMs, where model changes can alter not only posterior location and scale but also higher-order dependence, tail behavior, and local curvature.

There are, nevertheless, some limitations of our test-time training application in posterior inference of ABMs. First, our methods assumes simulator access at deployment and requires generating a (small) labeled target dataset, which may be expensive for highly complex simulators. Moreover, the update space of GradSubspace adaptation is identified locally around  $\phi_0$ , but if the target optimum lies far from the pre-trained solution, a single local subspace may be insufficient. Futhermore, the choice of subspace rank  $r$  and batching strategy ( $B$ ) introduces hyperparameters that may interact with simulator stochasticity and posterior multi-modality. Finally, since our evaluation only focuses on the Brock–Hommes model, validating the same stability gains across a broader class of ABMs remains necessary for a comprehensive account of generality.

Overall, this work establishes that test-time training is a practical and effective tool for fine-tuning normalizing-flow posteriors estimation of parameters in ABMs, and that objective-directed gradient subspaces can deliver both parameter efficiency and improved stability under distribution shift. Real-world ABMs deployments may involve more extreme, nonlocal shifts and tighter

simulation budgets, where a fixed, locally learned subspace and manually chosen ranks may limit adaptability. Future work should study adaptive rank selection and online subspace updates, layer or block-wise gradient subspaces that better match flow architecture, and broader evaluations on diverse ABMs to quantify reliability, calibration, and computational trade-offs in realistic implement settings.

## References

- [1] W. A. Brock and C. H. Hommes. Heterogeneous beliefs and routes to chaos in a simple asset pricing model. *Journal of Economic dynamics and Control*, 22(8-9):1235–1274, 1998.
- [2] Z. Cai, J. Tang, S. Mukherjee, J. Li, C.-B. Schönlieb, and X. Zhang. Nf-ula: Normalizing flow-based unadjusted langevin algorithm for imaging inverse problems. *SIAM Journal on Imaging Sciences*, 17(2):820–860, 2024.
- [3] D. Duan, R. Xu, P. Liu, and F. Wen. Lifelong test-time adaptation via online learning in tracked low-dimensional subspace. In *The Thirty-ninth Annual Conference on Neural Information Processing Systems (NeurIPS-2025)*, 2025.
- [4] J. Dyer, P. Cannon, J. D. Farmer, and S. M. Schmon. Black-box bayesian inference for agent-based models. *Journal of Economic Dynamics and Control*, 161:104827, 2024.
- [5] N. Gilbert. *Agent-based models*. Sage Publications, 2019.
- [6] J. Grazzini, M. G. Richiardi, and M. Tsionas. Bayesian estimation of agent-based models. *Journal of Economic Dynamics and Control*, 77:26–47, 2017.
- [7] E. J. Hu, Y. Shen, P. Wallis, Z. Allen-Zhu, Y. Li, S. Wang, L. Wang, W. Chen, et al. Lora: Low-rank adaptation of large language models. *ICLR*, 1(2):3, 2022.
- [8] G. Papamakarios and I. Murray. Fast epsilon-free inference of simulation models with bayesian conditional density estimation. In D. Lee, M. Sugiyama, U. Luxburg, I. Guyon, and R. Garnett, editors, *Advances in Neural Information Processing Systems*, volume 29. Curran Associates, Inc., 2016.
- [9] G. Papamakarios, E. Nalisnick, D. J. Rezende, S. Mohamed, and B. Lakshminarayanan. Normalizing flows for probabilistic modeling and inference. *Journal of Machine Learning Research*, 22(57):1–64, 2021.
- [10] S. Rajabi and S. Rambhatla. Optimizing fine-tuning efficiency: Gradient subspace tracking on grassmann manifolds for large language models. In *NeurIPS 2024 Workshop on Mathematics of Modern Machine Learning*, 2024.
- [11] D. Rezende and S. Mohamed. Variational inference with normalizing flows. In *International conference on machine learning*, pages 1530–1538. PMLR, 2015.
- [12] T. Shiono. Estimation of agent-based models using bayesian deep learning approach of bayesflow. *Journal of Economic Dynamics and Control*, 125:104082, 2021.
- [13] Y. Sun. *Test-Time Training*. PhD thesis, EECS Department, University of California, Berkeley, May 2023.

- [14] Y. Sun, X. Wang, Z. Liu, J. Miller, A. Efros, and M. Hardt. Test-time training with self-supervision for generalization under distribution shifts. In *International conference on machine learning*, pages 9229–9248. PMLR, 2020.
- [15] Z. Zhang, B. Liu, and J. Shao. Fine-tuning happens in tiny subspaces: Exploring intrinsic task-specific subspaces of pre-trained language models, 2023.

## A Additional Numerical Experiment on Multivariate Geometric Brownian Motion

### A.1 Multivariate Geometric Brownian Motion (MVGBM)

To further evaluate SNPE-TTT, SNPE-LoRA and Gradient-Based Test-Time Training, we conduct additional numerical experiments on Multivariate Geometric Brownian Motion (MVGBM), which is applied in a broad range of financial time-series modeling. This ABM is a continuous-time stochastic process with an analytically tractable discretised transition density. This makes it suitable for constructing a reliable likelihood-based reference posterior, serving as an additional sanity check under distribution shift.

We consider a  $d$ -dimensional positive-valued process  $X_t = (X_t^1, \dots, X_t^d) \in \mathbb{R}_+^d$ , whose components evolve according to the stochastic differential equation

$$dX_t^i = X_t^i \left[ \left( b_i - \frac{1}{2} \sum_{j=1}^d \sigma_{ij}^2 \right) dt + \sum_{j=1}^d \sigma_{ij} dW_t^j \right], \quad (19)$$

where  $b_i$  are drift coefficients,  $\sigma_{ij}$  are volatility coefficients, and  $\{W_t^j\}_{j=1}^d$  are components of a  $d$ -dimensional Brownian motion.

In this numerical experiment, we take  $d = 3$  and infer the posterior of  $\theta = (b_1, b_2, b_3)$ , given a discretely observed trajectory  $y \sim p(x \mid \theta^*)$  consisting of  $T = 100$  equally spaced time points with spacing  $\Delta t = 1/(T - 1)$ . We use independent uniform priors  $b_i \sim \mathcal{U}(-1, 1)$  for  $i = 1, 2, 3$ . To study the fine-tuning setting, we first train a base model under the above MVGBM setup using data generated with ground truth value  $\theta^* = (0.2, -0.5, -0.1)$ , and then fine-tune this base model by feeding it a small amount of new trajectory data from a shifted distribution with ground truth parameter  $\theta_{\text{new}}^* = (0.6, -0.5, -0.2)$ .

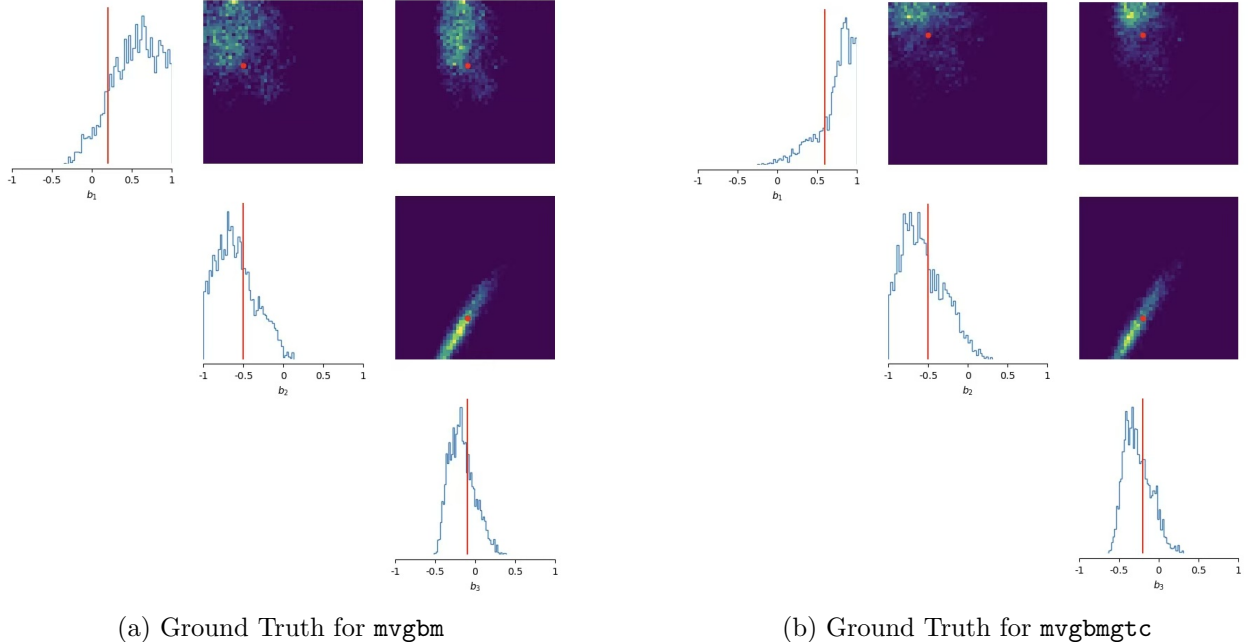


Figure 5: Ground truth posterior distributions

As the same as Brock-Hommes model, MVGBM is also likelihood-tractable thanks to a key property of its tractable transition density. Let  $Z_t = \log X_t$ , then

$$X_{t+\Delta t} = \exp Z_{t+\Delta t}, \quad Z_{t+\Delta t} \sim \mathcal{N}\left(\log X_t + (\theta - \gamma)\Delta t, \sigma\sigma^\top\Delta t\right), \quad (20)$$

where  $\exp(\cdot)$  denotes elementwise exponentiation and

$$\gamma = \frac{1}{2} \left[ \sum_{j=1}^d \sigma_{1j}^2, \sum_{j=1}^d \sigma_{2j}^2, \sum_{j=1}^d \sigma_{3j}^2 \right]^\top, \quad \sigma = \begin{pmatrix} 0.5 & 0.1 & 0.0 \\ 0.0 & 0.1 & 0.3 \\ 0.0 & 0.0 & 0.2 \end{pmatrix}. \quad (21)$$

Since the transition density in (20) is available in closed form, we can evaluate the likelihood numerically and obtain samples from an approximate ground-truth posterior using Metropolis–Hastings (MH), which is then used as a reference for assessing the effect of test-time training under distribution shift. The ground truth posterior distribution of two MVGBM settings generated by MH has been presented in Figure 5.

## A.2 Numerical Experiment for MVGBM

**Posterior Comparison** Figure 5 compares posterior samples from SNPE and other four test-time training approaches as we introduced in this work, SNPE-TTT, SNPE-LoRA, and the two objective-directed gradient-subspace variants GradSubspace-TTT and GradSubspace-PEA. As the same as results of previous numerical experiments in Brock-Hommes model shown in Figure 2, Figure 3 and Figure 4, the diagonal panels visualize marginal densities, the off-diagonal panels visualize pairwise joint structure and the vertical red lines indicate the ground-truth parameter values for visual calibration.

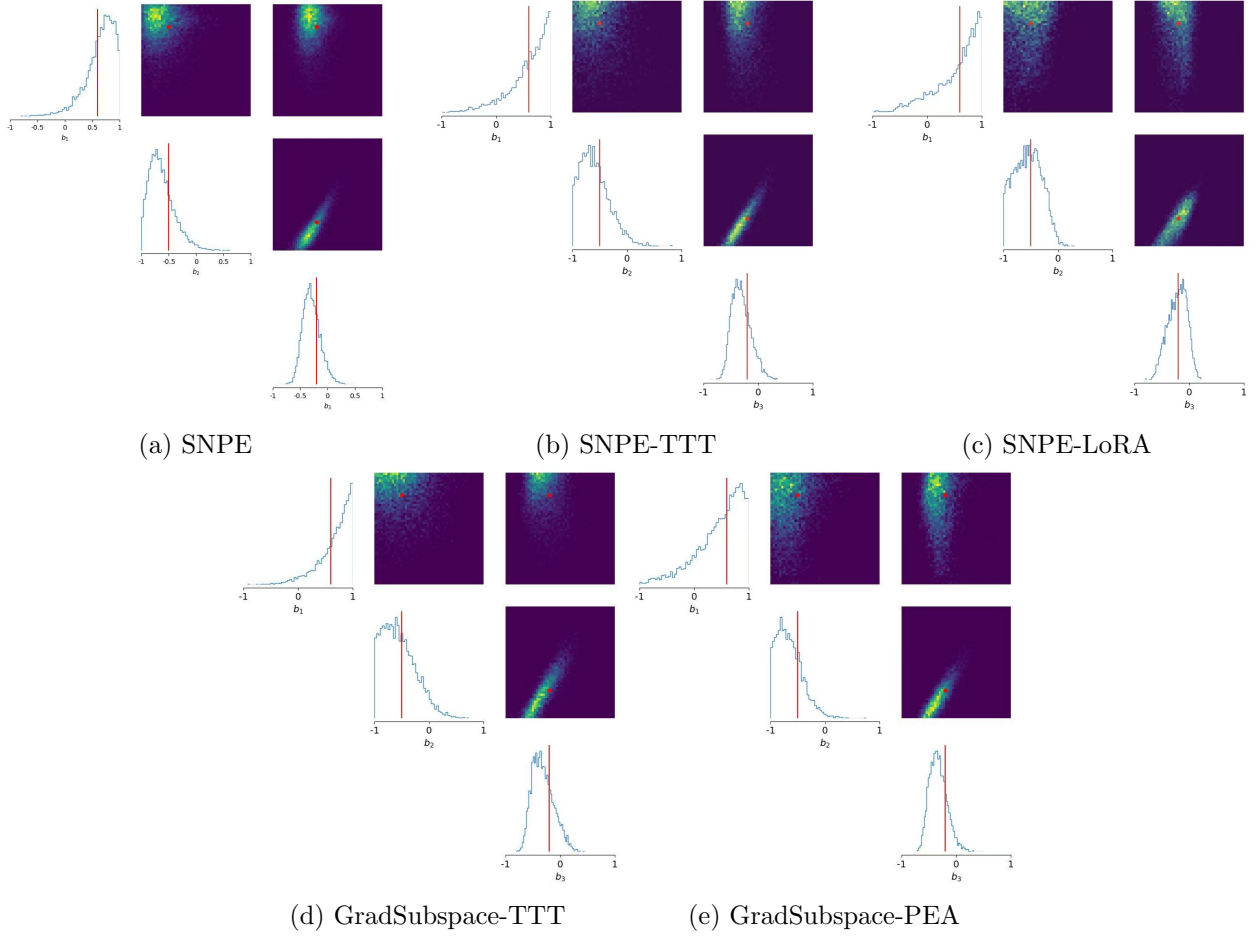


Figure 6: Posterior Comparison Between SNPE, SNPE-TTT, SNPE-LoRA, GradSubspace-TTT and GradSubspace-PEA for Numerical Experiment under MVGBM

While SNPE captures the dominant correlation patterns of the MVGBM posterior when compared against the ground-truth posterior, it exhibits visible bias in marginal locations. **SNPE-TTT** yields the most significant geometric correction, shifting both marginal modes and joint high-density regions toward the ground-truth posterior and thereby mitigating residual amortization gaps. **SNPE-LoRA** provides partial improvements by correcting some marginal shifts, yet it remains less consistent in matching the full joint dependence structure, plausibly due to its low-rank constraint. In contrast, **Gradient-Subspace** approaches preserve coherent joint geometry, particularly the dominant  $b_2$  and  $b_3$  correlation ridge, by confining updates to a target-gradient-informed subspace, effectively acting as an implicit regularizer against unconstrained drift.

**Discrepancy Comparison** As reported in Table 3, performance rankings vary by metric. In terms of Wasserstein distance (WASS), **SNPE-TTT** achieves the lowest discrepancy (0.0918), substantially outperforming the baseline (0.2601) and surpassing both SNPE-LoRA (0.1230) and GradSubspace-TTT (0.1088). However, GradSubspace-PEA shows limited gains (0.1595), suggesting its parameterization may be overly restrictive for reaching the ground-truth posterior under this shift. Conversely, SNPE yields the lowest MMD (0.0253), with test-time training methods showing slight increases. This divergence highlights that, relative to the ground-truth reference, test-time adaptation can improve global distributional alignment captured by WASS while simultaneously

altering finer-scale features measured by the kernel-based MMD. Overall, the results confirm that SNPE-TTT offers the most flexible correction toward the ground-truth posterior, while subspace methods provide stabilized, parameter-efficient alternatives.

Method	WASS	MMD
SNPE	0.2601	0.0253
SNPE-TTT	0.0918	0.0301
SNPE-LoRA	0.1230	0.0586
GradSubspace-TTT	0.1088	0.0720
GradSubspace-PEA	0.1595	0.0932

Table 3: Discrepancies between the approximate ground-truth posterior and the posteriors estimated with SNPE, classical Test-Time Training and GradSubspace variants under two metrics.